CDF Note 10775

Measurement of the W Boson Mass using 2.2 fb^{-1} of CDF II Data

The CDF Collaboration
URL http://www-cdf.fnal.gov

(Dated: February 23, 2012)

A measurement of the mass of the W boson, M_W, is presented using 2.2 fb^{-1} of data from $p\overline{p}$ collisions at $\sqrt{s} = 1.96$ TeV collected with the CDF II detector at the Fermilab Tevatron. The mass is determined by fitting simulated signal and background distributions to 470,126 W candidates decaying to $e\nu_e$ and 624,708 decaying to $\mu\nu_\mu$. The result is $M_W = 80387 \pm 19$ MeV and is the most precise determination of the mass to date.

Preliminary Result Winter 2011/12

I. INTRODUCTION

The mass of the W boson (M_W) is an important parameter of the standard model (SM). Precise measurements of M_W and of the top quark mass (m_t) significantly constrain the mass of the, as yet, unobserved Higgs boson. The current world average values of M_W (80399 ± 23 MeV) [1, 2] (not including this measurement) and $m_t(173.2 \pm 0.9$ GeV) [3], in conjunction with other electroweak data, determine the Higgs mass to be $m_H = 92^{+34}_{-26}$ GeV [4]. Measurements of M_W and m_t from the Tevatron, which dominate the world average, have currently only been made with a subset of the final Tevatron datasets which correspond to an integrated luminosity of $\sim$10 fb^{-1} per experiment.

The previous measurement of M_W by the CDF collaboration was determined to be $M_W = 80.413 \pm 0.048$ GeV [5] from only 200 pb^{-1} of data and a recent measurement by the DØ collaboration from 1 fb^{-1} of data gave $M_W = 80.401 \pm 0.043$ GeV [6]. In this note a measurement of M_W from 2.2 fb^{-1} of data is described. This supersedes the measurement in Ref. [5].

At the Tevatron, W bosons are primarily produced in $q\bar{q}$ annihilation, $q\bar{q} \rightarrow W + X$, where X can include QCD radiation that results in measurable hadronic recoil in events. $W \rightarrow l\nu_l$ decays, where $l = e$ or μ, are selected with high purity by the CDF detector and used to measure M_W. The final-state kinematics of W candidates cannot be fully reconstructed since the longitudinal momentum of the neutrino is not measured. Thus, in order to extract M_W, transverse [7] components of charged lepton momentum (p_T^l), neutrino momentum (p_T^ν) and the transverse mass,

$$m_T = \sqrt{2p_T(l)p_T(\nu)[1 - cos(\phi_l - \phi_\nu)]}, \tag{1}$$

are used which depend only on measurable quantities of the W decay. A Monte Carlo simulation is used to predict the shape of these distributions as a function of M_W. A binned maximum-likelihood fit of these predictions to the data is used to determine the W boson mass.

These line-shape predictions depend on the kinematic distributions of the W decay products and detector effects, which are constrained from control samples and theoretical calculations. The kinematic distributions are determined by several effects including internal QED radiation, the intrinsic W boson transverse momentum, and the proton parton distribution functions (PDFs). Detector effects include external bremsstrahlung and ionisation energy loss in the detector material, tracker momentum scale, calorimeter energy scale, resolutions of the tracker and calorimeter, and the detector acceptance. A sophisticated, fast simulation has been developed that enables a study of these effects at a level below 1 part in 10^4.

In the following sections the components of the W boson mass measurement: event generation (including next-to-leading-order photon and gluon radiation), detector simulation, event selection, calibration of detector energy and momentum scales, calibration of the hadronic recoil measured in the calorimeter and background determination are described and the corresponding systematic uncertainties detailed.

II. CDF DETECTOR

The CDF II detector is a multipurpose detector consisting of an inner silicon tracker designed to measure the production vertex of charged particles with high precision, an outer tracking drift chamber, the COT, to measure charged particle momenta, a solenoid to provide a uniform 1.4 T magnetic field inside the trackers, electromagnetic calorimeters to contain and measure electron and photon showers, hadronic calorimeters for hadron energy measurements, and a muon system to detect muons escaping the calorimeter. A three-level trigger system, that has high efficiency for W and Z bosons, is used to initially select the candidate events.

III. EVENT GENERATION

W events are generated with the RESBOS Monte Carlo [8], which captures the relevant QCD physics and models the W p_T spectrum. This is coupled with PHOTOS [9], which accounts for the relevant QED processes. PHOTOS also includes leading-log calculations of electroweak processes, including multiple, real, final-state photons. This QED radiation model is cross-checked against HORACE [10] which, in addition to a leading-log calculation of multiple initial and final-state photons, also performs an exact $\mathcal{O}(\alpha)$ calculation for single photons. Uncertainties in the QED radiation modelling, including the choice of generator, the choice of the minimum photon energy, the effect of soft and virtual corrections, and $\gamma \rightarrow e^+e^-$ splitting, result in an uncertainty in M_W of 4 MeV for all three fits in both the electron and muon channels.

The W p_T spectrum has a significant impact on the simulated p_T line-shapes and is thus an important ingredient of the W boson mass measurement. This spectrum is modeled using RESBOS, which computes the quintuple differential cross section $\frac{d^5\sigma}{dQ_T^W\, dy_W\, dQ_W^2\, d\Omega}$ for $p\bar{p} \to W^{\pm}$. RESBOS models the W p_T spectrum at low p_T via multiple-soft-gluon re-summation techniques. The non-perturbative physics is described by parameters that must be determined from experimental data. In this analysis the three parameter (g_1, g_2, g_3) model of [11, 12] is used. g_2 predominantly determines the shape of the boson p_T spectra at the Tevatron beam energy and is determined from a fit to the dilepton spectra of $Z \to ee$ and $Z \to \mu\mu$ candidate events with an uncertainty of 0.013 GeV^2. Uncertainties in g_1, g_3 from [12] and in α_s from [13], and their correlation with g_2 are also considered. The g_2 uncertainty dominates and the resulting systematic uncertainty in M_W from the W p_T modelling is 3 MeV, 9 MeV, and 4 MeV for the m_T, p_T^l, and p_T^{ν}, fits, respectively.

PDFs affect the W boson mass measurement through their effects on the kinematics of the decay charged lepton and because the measurement only uses charged leptons in a restricted rapidity range. The uncertainty arising from the PDFs is evaluated using the 68% C.L MSTW2008 [14] error set. This is cross-checked by comparing the 90% C.L. CTEQ6.6 [15] error set with the 90% C.L MSTW2008 error set. The uncertainty in M_W, for both electron and muon channels, are 10 MeV for the m_T fit, 9 MeV for the charged lepton p_T fit, and 11 MeV for the neutrino p_T fit. Within these errors the CTEQ6.6 and MSTW2008 sets are in agreement. The CTEQ6.6 PDF is used in the final M_W determination.

IV. DETECTOR SIMULATION

The tracker and calorimeter response and the electron and muon acceptance are simulated using a parameterized fast detector simulation. Tracks in the COT associated with electrons and muons are simulated at the hit level. Electrons and muons are propagated along a helical trajectory from the production point, stepping through the layers of passive material, whose effects are simulated. The most relevant processes are ionisation energy loss for muons, bremsstrahlung ($e \to e\gamma$) for electrons, and conversion ($\gamma \to e^+e^-$) for photons. Multiple Coulomb scattering is simulated in order to incorporate its effect on track resolution.

The deposition of electromagnetic energy in the calorimeter for leptons and photons is simulated using parameterizations for the energy scale and resolution; energy loss in the solenoidal coil and due to longitudinal leakage; and non-linear response. The parameters for the scale and resolution, and the non-linearity, are fit from the data.

V. EVENT SELECTION

The event selection criteria for the W boson mass measurement are optimized to produce a sample with low background and which can be accurately modeled. W and Z boson candidates are selected by requiring the charged leptons have p_T greater than 30 GeV. Muon candidates are required to have hits in the muon detectors and electron candidates must have an E/p value of less than 1.6. Additionally two leptons of the same flavor and opposite charge as well as the mass of the dilepton system to be in the range $66 < m_{ll} < 116$ GeV are required for Z candidates. For W boson candidates, the recoil energy in the calorimeter is required to be less than 15 GeV, $\not\!\!E_T > 30$ GeV and $60 < m_T < 100$ GeV. These selection criteria are applied to data collected between February 2002 and September 2007. The data correspond to an integrated luminosity of 2.2 fb^{-1}. The selection criteria yield 470,126 $W \to e\nu$ candidates and 624,708 $W \to \mu\nu$ candidates.

VI. MOMENTUM SCALE CALIBRATION

The high statistics $J/\psi \to \mu\mu$ and $\Upsilon(1S) \to \mu\mu$ quarkonia decays, along with the $Z \to \mu\mu$ sample, are used to set the momentum scale. The momentum scale is extracted from a binned maximum likelihood fit of the data to simulated invariant mass templates generated using the world average values.

The J/ψ sample has the advantage that its cross section is sufficiently large to enable a study of the momentum scale as a function of other variables. The $\Upsilon(1S)$ resonance has an invariant mass three times larger than the J/ψ, and supplies an intermediate reference point to study the momentum dependence of the momentum scale. The Υ hadrons also have the advantage that they are all produced promptly, allowing a study of the momentum scale using tracks that are beam-constrained in the same way as the tracks in the W and Z samples.

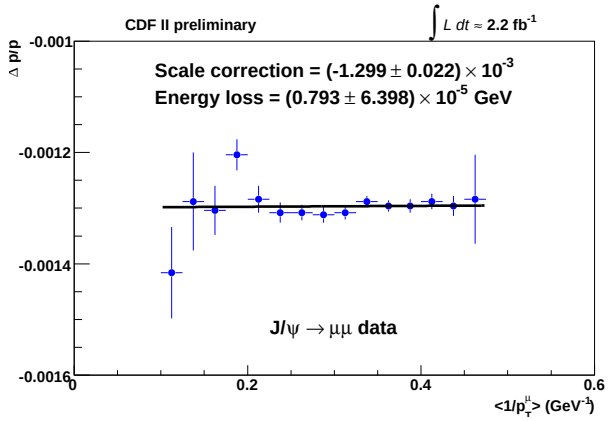

FIG. 1: The fractional momentum correction for data as a function of the mean inverse momentum of muons from J/ψ decay.

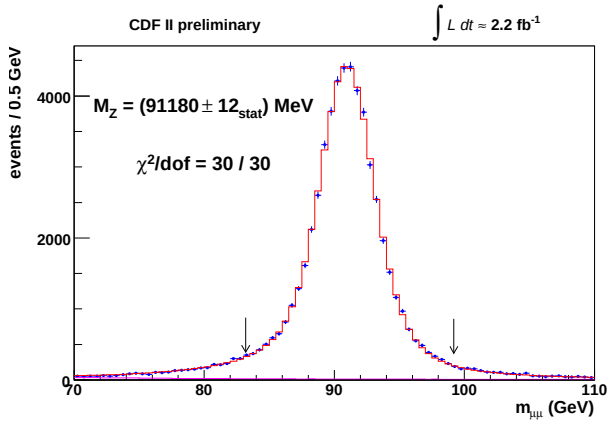

FIG. 2: The fitted $Z \to \mu\mu$ mass using the COT momentum scale derived from the $J/\psi \to \mu\mu$ and $\Upsilon \to \mu\mu$ measurements. The data (points) are shown along with the best-fit simulation template (histogram). The arrows indicate the fitting range.

The momentum scale is calibrated after alignment and energy loss corrections are derived from the J/ψ sample. Non-uniformities in the tracker magnetic field are corrected by removing the dependence of the J/ψ mass on the mean polar angle of the muons. An observed scale dependence on the polar angle difference of the two muon tracks is eliminated by correcting the track curvature and scaling the track polar angle. Finally, the scale dependence on the mean inverse muon p_T is eliminated by scaling the tracker material as shown in Fig. 1. The combined momentum scale obtained from the J/ψ and Υ samples is applied to the W and Z samples.

The $Z \to \mu\mu$ mass fit is shown in Fig. 2, along with the statistical uncertainty and fit χ^2. A value of $m_Z = 91180 \pm 12_{stat} \pm 10_{syst}$ MeV is obtained, consistent with the world average value of $m_Z = 91188 \pm 2$ MeV [16]. Combining the J/ψ, Υ, and Z measurements, yields an overall momentum scale

$$\Delta p/p = (-129 \pm 9) \times 10^{-5}, \tag{2}$$

which is applied to the W boson data in both electron and muon channels. A measurement of the Z boson mass using only track momenta of $Z \to ee$ decays is found to be in good agreement with the $Z \to \mu\mu$ measurement and validates the application of the tracker momentum scale to electrons. The resulting tracker momentum scale uncertainty is 7 MeV on M_W in the muon channel. The momentum scale uncertainty is the same for the m_T, p_T^l and p_T^ν, fits as it is a global multiplicative factor in all measurements.

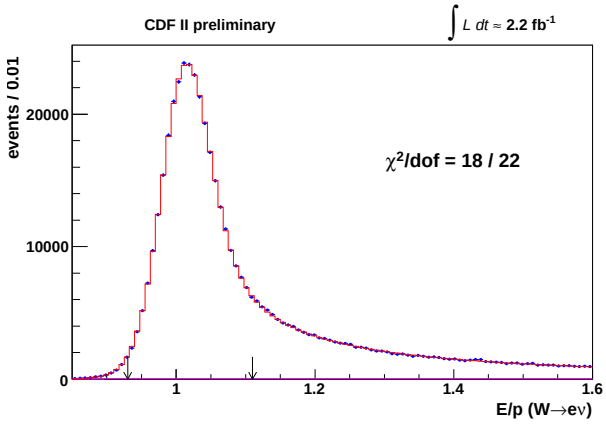

FIG. 3: The E/p distribution of the $W \to e\nu$ data (points) used to determine the calorimeter energy scale. The arrows indicate the fitting range used for the electron energy calibration.

VII. ENERGY SCALE CALIBRATION

The electron cluster is simulated by merging energies of the primary electron and proximate bremsstrahlung photons and conversion electrons. The distribution of electron and photon energy loss in the solenoid coil and leakage into the hadronic calorimeter are determined using GEANT.

The electromagnetic calorimeter energy scale is set using the peak of the E/p electron distribution from $W \to e\nu$ events (Fig. 3) and $Z \to ee$ events. A fit in the peak region of $0.93 < E/p < 1.11$ is performed. Consistent results are obtained from the W and Z samples enabling the results to be combined to define the overall scale to a precision better than 0.01%. The electromagnetic calorimeter non-linearity is determined from E/p fits as a function of transverse energy from the $W \to e\nu$ and $Z \to ee$ samples. The tail of the E/p distribution is used to tune the absolute number of radiation lengths in the tracker material, as shown in Fig. 4. The electromagnetic calorimeter resolution is parameterized as:

$$\sigma_E/E = 12.6\%/\sqrt{E_T} \oplus \kappa, \tag{3}$$

where κ is the non-stochastic term in the resolution. Two κs are defined. The first, κ_e, defines the smearing of the primary high-E_T electron and is tuned from the peak region of the E/p distribution. The second, κ_γ, smears the energy contribution of each of the secondary electromagnetic particles: the bremsstrahlung photons and the conversion electrons. κ_γ is tuned on the width of the $Z \to ee$ distribution selected using high E/p ($E/p > 1.06$) electrons.

The $Z \to ee$ mass is fitted to cross-check the energy scale and the non-linearity (Fig. 5). A value of $m_Z = 91230 \pm 30_{stat} \pm 14_{syst}$ MeV is obtained, consistent with the world average. Thus, the measurements from E/p and the $Z \to ee$ mass are combined to obtain the most precise energy scale. Combining the uncertainties from the calorimeter energy scale calibration, the uncertainties on the electron m_T, p_T^l, and p_T^ν, fits are 10 MeV each. Of this uncertainty, 5 MeV is taken to be correlated with the muon channel through the momentum scale uncertainty.

VIII. RECOIL CALIBRATION

All particles recoiling against the W or Z boson are collectively referred to as the recoil. The recoil vector $\mathbf{u}$ is defined as the vector sum of transverse energy over all electromagnetic and hadronic calorimeter towers in the detector range $|\eta| < 2.4$. The calorimeter towers associated with the leptons are explicitly removed from the recoil calculation. A combination of minimum bias data and $Z \to ll$ data is used to model the behavior of the hadronic recoil, and $W \to l\nu$ data is used to cross-check the data corrections and the simulation.

The response of the calorimeter to the hadronic recoil is described by a response function, R, which scales the true recoil magnitude to simulate the measured magnitude. The response function is parameterized as

$$R \equiv u_{rec}/u_{true} = a \log(u_{true} + b)/\log(15 + b), \tag{4}$$

where u_{true} is the true recoil magnitude and u_{rec} is the reconstructed recoil magnitude. This logarithmic function describes a monotonically increasing response, with a equal to the value of the response at $u_{true} = 15$ GeV, and b

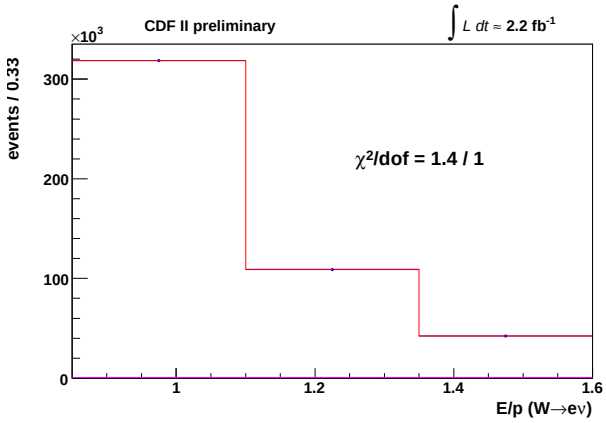

FIG. 4: The electron E/p distribution of the $W \to e\nu$ data used for scaling radiative material in the simulation. The first (peak) bin is used to determine normalisation while the remaining two bins are used for tuning.

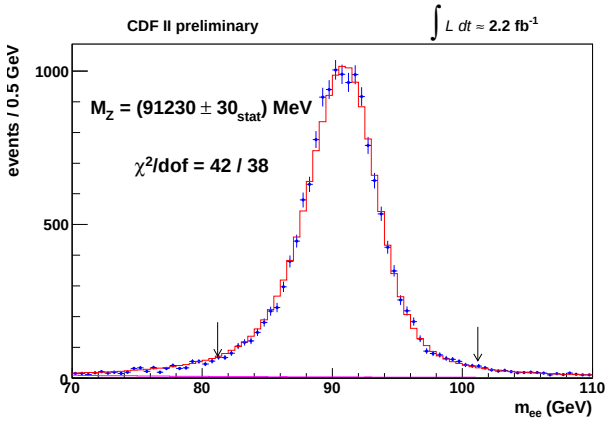

FIG. 5: The maximum likelihood fit to the $Z \to ee$ mass peak, with the fitted mass value. The data (points) are shown along with the best-fit simulation template (histogram). The arrows indicate the fitting range.

describing the variation of the response with u_{true}. The pivot point at 15 GeV is chosen such that the parameters a and b are uncorrelated in their fit to the Z boson data.

The recoil resolution is assumed to have two components, which are summed vectorially: a "sampling" term representing the calorimeter "jet" resolution, and an underlying event component from the spectator and additional $p\bar{p}$ interactions. The sampling resolution is parameterized as $s_{had} \cdot \sqrt{u_{true}}$ and the underlying event contribution is represented by a random vector (e_x, e_y), given by

$$e_i = A_i + B_i \cdot \Sigma E_T \oplus \sigma_i(\Sigma E_T). \tag{5}$$

The mean values of e_x and e_y are separately parameterized as linear functions of ΣE_T from minimum-bias data.

$Z \to \mu\mu$ and $Z \to ee$ events are used to tune the recoil response and resolution parameters. The η axis is defined to be the geometric bisector of the two leptons and the ξ axis to be perpendicular to η. The vector p_T-balance $(\vec{p}_T + \vec{u})$ is projected onto the η and ξ axes, and data distributions are compared to the simulation. The hadronic scale parameters a and b in Eq. 4 are tuned using the mean value of the p_T-balance in the η direction, as a function of $p_T(ll)$. These distributions, after tuning, are shown in Fig. 6 for both $Z \to ee$ and $Z \to \mu\mu$. The resolution parameters are measured by comparing the RMS of the p_T-balance in the η and ξ directions, again as a function of $p_T(ll)$. These distributions, after tuning, are shown in Figs. 7 and 8.

The systematic uncertainty on the W boson mass due to the recoil scale is determined by varying R through the statistical uncertainties on the parameters a and b. The uncertainties for the m_T, p_T^l, and p_T^ν, fits are 5 MeV, 6 MeV, and 2 MeV, respectively. Varying the two recoil resolution parameters by their uncertainties results in M_W uncertainties of 7 MeV, 5 MeV and 11 MeV for the m_T, p_T^l and p_T^ν fits, respectively. These uncertainties apply to both electron and muon channels.

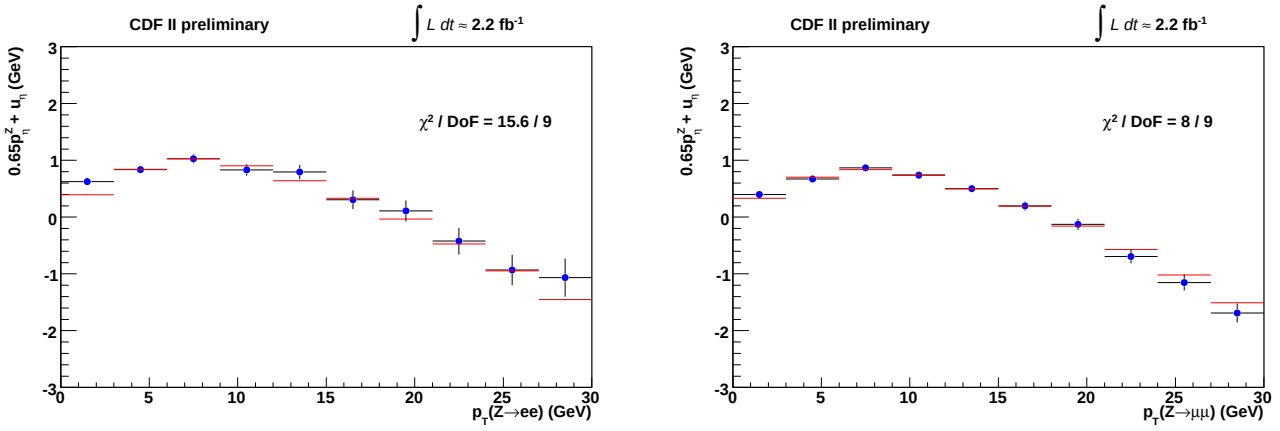

FIG. 6: Mean value of the scaled p_T-balance projected onto the η axis as a function of p_T(ll) for $Z \to ee$ (left) and $Z \to \mu\mu$ (right).

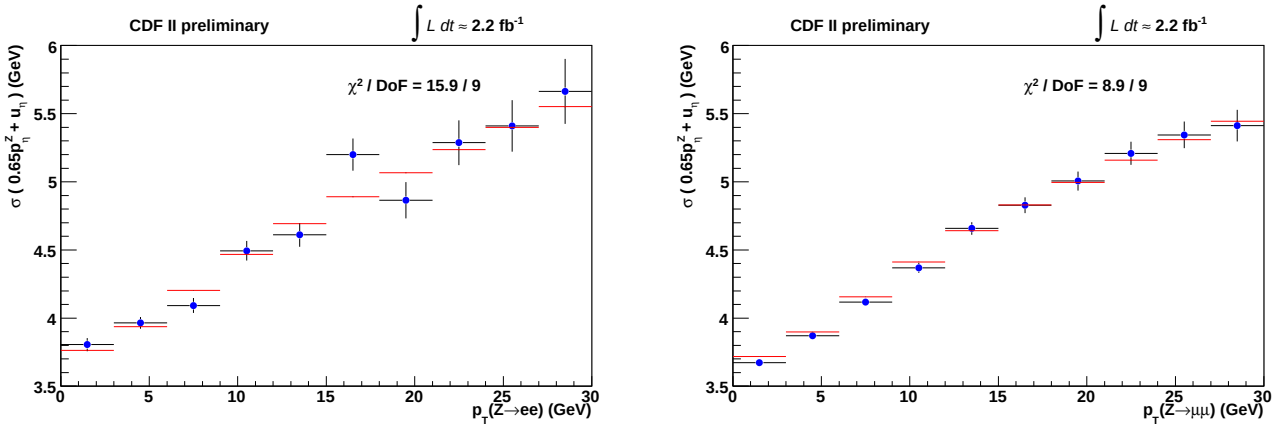

FIG. 7: RMS of the scaled p_T-balance projected onto the η axis as a function of p_T(ll) for $Z \to ee$ (left) and $Z \to \mu\mu$ (right).

IX. BACKGROUND MEASUREMENT

Backgrounds passing the event selection cuts have different kinematic distributions from the W signal, and are therefore included in the template fits. The backgrounds to the $W \to \mu\nu$ and $W \to e\nu$ samples come from hadronic jet production, decays in flight, Z production, $W \to \tau\nu$ decays, and cosmic rays.

The electroweak backgrounds originating from $Z \to ll$ decays are estimated using Monte Carlo samples generated with PYTHIA and simulated with the GEANT detector simulation. Backgrounds originating from $W \to \tau\nu$ are modeled in the parameterized fast simulation and cross-checked using GEANT simulated PYTHIA Monte Carlo. The other backgrounds are characterized using the data. The jet background is estimated using a neural network trained with W Monte Carlo as signal and QCD-enriched data as background. Decays-in-flight (DIF) of kaon and pion particles typically have poorly reconstructed COT tracks and can be mostly rejected using their abnormal COT hit pattern and large track fit χ^2. The remaining DIF are evaluated with a fit to the track χ^2 distribution. The cosmic ray background is estimated by studying the t_0 of the reconstructed muon track. Background fractions for the muon (electron) datasets are evaluated to be 7.35% (0.14%) from Z decays, 0.88% (0.93%) from $W \to \tau\nu$ decays, 0.04% (0.39%) from hadronic jets, 0.24% from DIF, and 0.02% from cosmic rays. The systematic uncertainty due to backgrounds is estimated to be 3 MeV and 4 MeV in the m_T fit for the muon and electron channels respectively. The corresponding uncertainties for the p_T^l (p_T^ν) fits are 5 MeV (6 MeV) and 3 MeV (4 MeV).

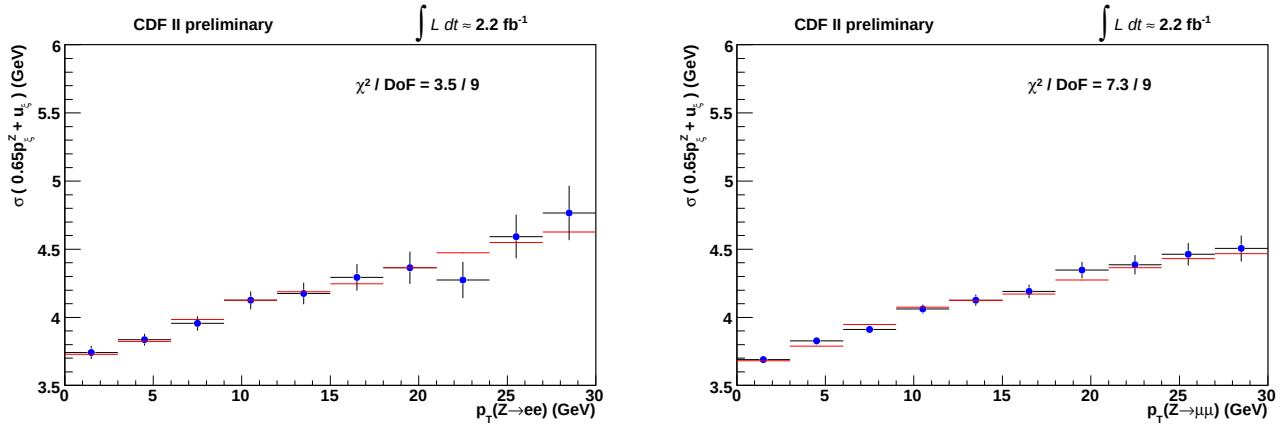

FIG. 8: RMS of the scaled p_T-balance projected onto the ξ axis as a function of p_T(ll) for $Z \to ee$ (left) and $Z \to \mu\mu$ (right).

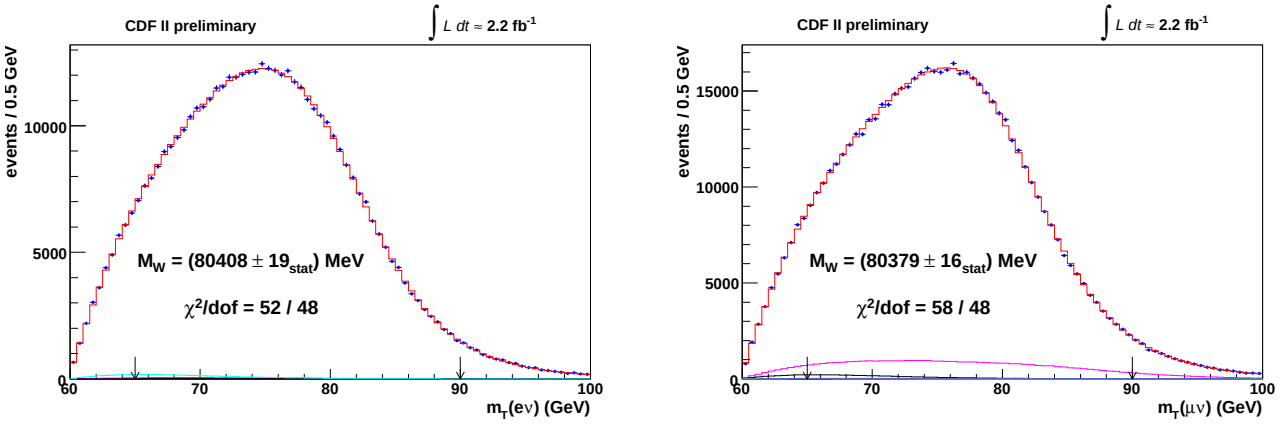

FIG. 9: The W transverse mass fits for the electron (left) and muon (right) channels. The data (points) are shown along with the best-fit simulation template (red histogram). The background contributions to the template, including $Z \to ll$ (magenta histogram) and hadronic jets (cyan histogram), are overlaid. The arrows indicate the fitting range.

X. MASS FITS AND RESULTS

The W boson mass is measured by performing a binned maximum-likelihood fit to the lepton p_T, neutrino p_T, and m_T distributions for each lepton channel. 1600 signal templates for M_W are generated between 80 GeV and 81 GeV and background templates are added with the shapes and normalisations described in Sec. IX. The final fit values were hidden during analysis by adding an unknown offset in the range [-75,75] MeV. The results of the fits to the m_T, p_T^l, and p_T^ν kinematic distributions for both the electron and muon channels are summarized in Table I.

Figures 9, 10, and 11 show the mass fits for the transverse mass, charged lepton p_T, and neutrino p_T distributions, respectively, in both the electron and muon samples. The fit regions are 65 GeV $< m_T <$ 90 GeV and 32 GeV $< p_T^l$, $p_T^\nu <$ 48 GeV.

Tables II-IV list the systematic uncertainties of the three fits, including the correlated uncertainties between electrons and muons.

Fits of simulated data to Monte Carlo templates have been performed to measure the statistical correlation between the fits to the m_T, p_T^l and p_T^ν distributions. The statistical correlations between the m_T and p_T^l fits is determined to be 70.9 ± 2.5 % (67.2 ± 2.8 %) and those between the m_T and p_T^ν fits to be 69.4 ± 2.6 % (65.8 ± 2.8 %) in the electron (muon) channels. The electron (muon) channel p_T^l and p_T^ν fits are 30.7 ± 4.5 % (25.5 ± 4.7 %) correlated. The systematic uncertainties listed as common in Tables II-IV are assumed to be 100% correlated between channels. The Best-Linear-Unbiased-Estimator (BLUE) [17] method is used to combine the different W boson mass fits, calculating a full covariance matrix for statistical and systematic uncertainties in all fits.

With the systematic uncertainties quoted in Tables II-IV and the statistical precisions from Table I, the combined

Charged Lepton	Kinematic Distribution	Fit Result (MeV)	χ^2/DoF
Electron	Transverse mass	80408 ± 19	52/48
Electron	Charged lepton p_T	80393 ± 21	60/62
Electron	Neutrino p_T	80431 ± 25	71/62
Muon	Transverse mass	80379 ± 16	57/48
Muon	Charged lepton p_T	80348 ± 18	58/62
Muon	Neutrino p_T	80406 ± 22	82/62

TABLE I: Fit results and statistical errors for electrons and muons from the three kinematic distributions used to extract M_W.

Systematic (MeV)	Electrons	Muons	Common
Lepton Energy Scale	10	7	5
Lepton Energy Resolution	4	1	0
Recoil Energy Scale	5	5	5
Recoil Energy Resolution	7	7	7
$u_{\|\|}$ Efficiency	0	0	0
Lepton Removal	3	2	2
Backgrounds	4	3	0
$p_T(W)$ Model (g_2, g_3, α_s)	3	3	3
Parton Distributions	10	10	10
QED Radiation	4	4	4
Total	18	16	15

TABLE II: Table of systematic uncertainties for the transverse mass fits.

Systematic (MeV)	Electrons	Muons	Common
Lepton Energy Scale	10	7	5
Lepton Energy Resolution	4	1	0
Recoil Energy Scale	6	6	6
Recoil Energy Resolution	5	5	5
$u_{\|\|}$ efficiency	2	1	0
Lepton Removal	0	0	0
Backgrounds	3	5	0
$p_T(W)$ model (g_2, g_3, α_s)	9	9	9
Parton Distributions	9	9	9
QED radiation	4	4	4
Total	19	18	16

TABLE III: Table of systematic uncertainties for the charged lepton p_T fits.

Systematic (MeV)	Electrons	Muons	Common
Lepton Energy Scale	10	7	5
Lepton Energy Resolution	7	1	0
Recoil Energy Scale	2	2	2
Recoil Energy Resolution	11	11	11
$u_{\|\|}$ efficiency	3	2	0
Lepton Removal	6	4	4
Backgrounds	4	6	0
$p_T(W)$ model (g_2, g_3, α_s)	4	4	4
Parton Distributions	11	11	11
QED radiation	4	4	4
Total	22	20	18

TABLE IV: Table of systematic uncertainties for the missing transverse energy fits.

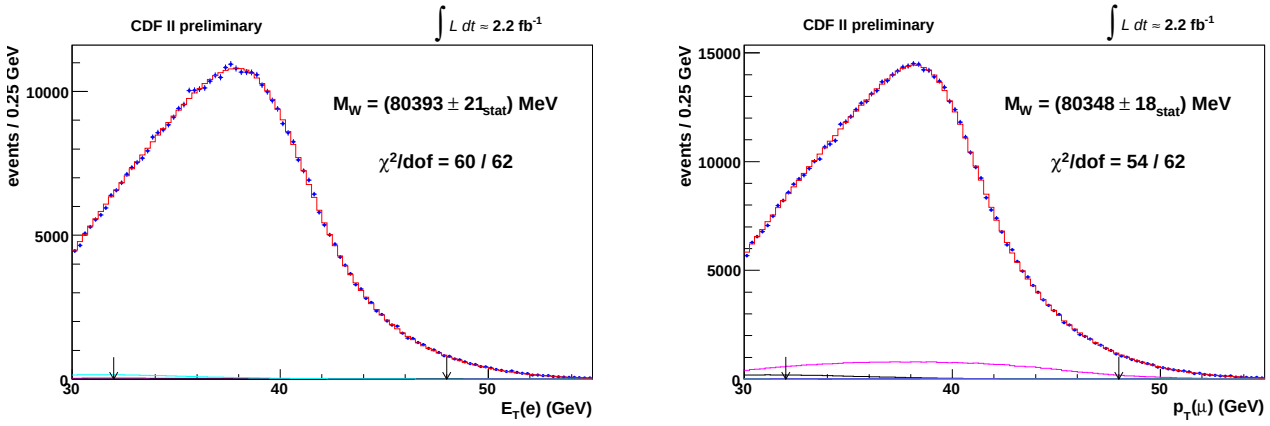

FIG. 10: The charged lepton p_T fits for the electron (left) and muon (right) channels. The data (points) are shown along with the best-fit simulation template (red histogram). The background contributions to the template, including $Z \to ll$ (magenta histogram) and hadronic jets (cyan histogram) are overlaid. The arrows indicate the fitting range.

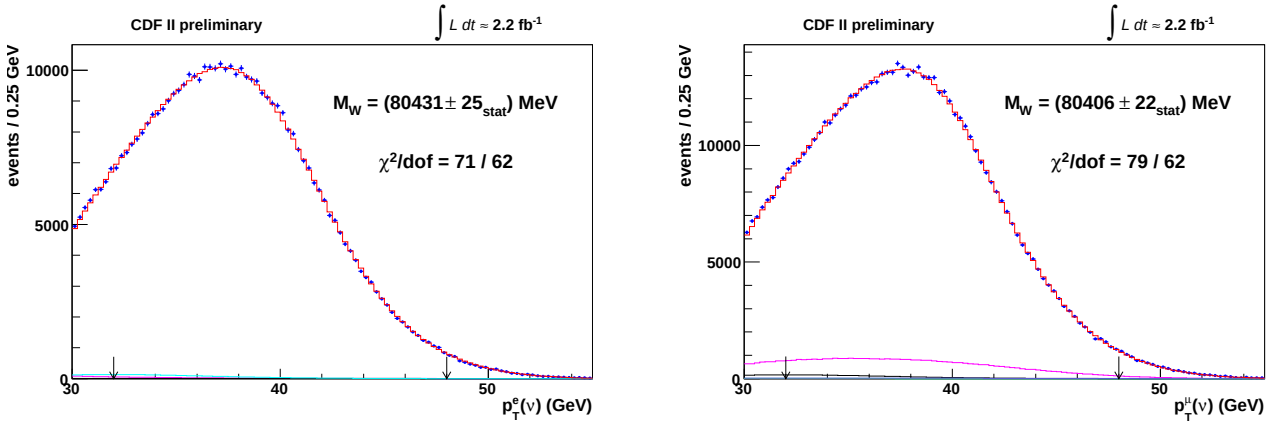

FIG. 11: The neutrino p_T fits for the electron (left) and muon (right) channels. The data (points) are shown along with the best-fit simulation template (red histogram). The background contributions to the template, including $Z \to ll$ (magenta histogram) and hadronic jets (cyan histogram) are overlaid. The arrows indicate the fitting range.

mass value from the transverse mass fits is:

$$M_W = 80390 \ \pm 20 \ \text{MeV}$$

This combination yields $\chi^2 = 1.2$ /1 with a probability of 28 %. This probability tests the compatibility of the electron and muon channels.

The combination of the charged lepton p_T fits gives:

$$M_W = 80366 \ \pm 22 \ \text{MeV}$$

This combination yields $\chi^2 = 2.3$ /1 with a probability of 13 %.

The combination of the neutrino p_T fits gives:

$$M_W = 80416 \ \pm 25 \ \text{MeV}$$

This combination yields $\chi^2 = 0.5$ /1 with a probability of 49 %.

The combination of the m_T, p_T^l and p_T^ν, fits for the electron channel gives:

$$M_W = 80406 \ \pm 25 \ \text{MeV}$$

This combination yields $\chi^2 = 1.4$ /2 with a probability of 49 %.

The combination of the m_T, p_T^l and p_T^ν, fits for the muon channel gives:

$$M_W = 80374 \ \pm 22 \ \text{MeV}$$

This combination yields $\chi^2 = 4$ /2 with a probability of 12 %.
The combination of the m_T, p_T^l and p_T^ν, fits for the electron and muon channels gives:

$$M_W = 80387 \ \pm 19 \ \text{MeV}$$

This combination yields $\chi^2 = 6.6$ /5 with a probability of 25 %. Compared to the combination of the two m_T fits alone, the combination of all 6 fits results in a reduction of the total uncertainty by 1 MeV.

XI. CONCLUSIONS

The W boson mass has been determined from fits to the transverse mass, charged lepton transverse momentum and neutrino transverse momentum distributions of $W \to e\nu$ and $W \to \mu\nu$ decays. Combining all six mass results, M_W is measured to be

$$M_W = 80387 \pm 19 \text{ MeV}$$

from 2.2 fb^{-1} of CDF Run II data. This measurement represents the most precise M_W measurement to date.

Using the procedure defined by the Tevatron Working Group [2] to combine this result with previous (Run-0/I) CDF measurements and (Run-I/II) DØ measurements results in a Tevatron M_W of 80394 ± 18 MeV, dominated by the result presented here. Assuming no correlation with the LEP M_W (80376 ± 33 MeV) determination, a new world average of $M_W = 80390 \pm 16$ MeV is determined. This results in a new Higgs mass estimate of $m_H = 90^{+29}_{-23}$ GeV [18] and an upper bound on m_H of 145 GeV at 95% C.L.

Acknowledgments

We thank the Fermilab staff and the technical staffs of the participating institutions for their vital contributions. This work was supported by the U.S. Department of Energy and National Science Foundation; the Italian Istituto Nazionale di Fisica Nucleare; the Ministry of Education, Culture, Sports, Science and Technology of Japan; the Natural Sciences and Engineering Research Council of Canada; the National Science Council of the Republic of China; the Swiss National Science Foundation; the A.P. Sloan Foundation; the Bundesministerium für Bildung und Forschung, Germany; the Korean World Class University Program, the National Research Foundation of Korea; the Science and Technology Facilities Council and the Royal Society, UK; the Russian Foundation for Basic Research; the Ministerio de Ciencia e Innovación, and Programa Consolider-Ingenio 2010, Spain; the Slovak R&D Agency; the Academy of Finland; and the Australian Research Council (ARC).

[1] $c = 1$ is used throughout.
[2] Tevatron Electroweak Working Group, `http://arxiv.org/abs/0908.1374`.
[3] Tevatron Electroweak Working Group, `http://arXiv.org/abs/1107.5255`.
[4] LEP Electroweak Working Group, `http://lepewwg.web.cern.ch/LEPEWWG/`, and references therein.
[5] T. Aaltonen *et. al.* Phys. Rev. Lett. **99**, 151801 (2007).
[6] V. Abazov *et. al.* Phys. Rev. Lett. **103**, 141801 (2009).
[7] CDF uses a cylindrical coordinate system with the z axis along the proton beam axis. Pseudorapidity is $\eta \equiv -\ln(\tan(\theta/2))$, where θ is the polar angle, and ϕ is the azimuthal angle relative to the proton beam direction, while $p_T = |p| \ \sin(\theta)$, $E_T = E \ \sin(\theta)$.
[8] C. Balazs and C.-P. Yuan, Phys. Rev. D **56** 5558 (1997).
[9] E. Barberio and Z. Was, Comp. Phys. Commun. **79**, 291 (1994).
P. Golonka and Z. Was, Eur. J. Phys. C **45**, 97 (2006).
[10] C.M. Carloni Calame *et. al.*, JHEP **0710**, 109 (2007).
[11] G. A. Ladinsky and C.-P. Yuan, Phys. Rev. D **50**, 4239 (1994).

[12] F. Landry, R. Brock, P.M. Nadolsky, C.-P. Yuan, Phys. Rev. D **67** 073016 (2003).
[13] A.D. Martin, W.J. Stirling, R.S. Thorne, G. Watt, Eur. Phys. J. C **64** 653 (2009).
[14] A.D. Martin, W.J. Stirling, R.S. Thorne, G. Watt, Eur. Phys. J. C **63** 189 (2009).
[15] J. Pumplin, D. Stump, J. Huston, H-L. Lai, P. Nadolsky, W-K. Tung, J. High Energy Phys. **07**, 012 (2002).
[16] The ALEPH, DELPHI, L3, OPAL, SLD Collaborations, Physics Reports **427** 257 (2006).
[17] L. Lyons, D. Gibaut, and P. Clifford, Nucl. Instr. Meth. A **270**, 110 (1988).
[18] Private Communication Peter Renton (for the LEP EWK Working Group).